Global Exploration of the Enthalpy Landscape of Calcium Carbide

A. Kulkarni, K. Doll,* J. C. Schön, and M. Jansen

Max Planck Institute for Solid State Research, Heisenbergstr. 1, D-70569 Stuttgart, Germany

Received: March 30, 2010; Revised Manuscript Received: August 2, 2010

The enthalpy landscape of CaC_2 was investigated on the ab initio level, and possible (meta)stable structures are predicted. Simulated annealing was used as a global exploration method for the determination of the local minima on the enthalpy landscapes, where the only information supplied was the number of atoms per unit cell. Subsequently, the structure candidates found were locally optimized. At all stages of the search, the energy calculations were performed on the ab initio level. Furthermore, we investigated the enthalpies of different modifications as a function of pressure, and we found that, at a transition pressure of about 30 GPa, CaC_2 should transform from a 6-fold coordinated structure resembling a rock-salt structure to an 8-fold coordinated one similar to the CsCl structure. At standard pressure, two new energetically low-lying (metastable) structures were found, and at high pressure an additional new metastable structure was also predicted to be capable of existence.

Introduction

One of the major goals in theoretical solid-state chemistry is the development of a methodology to predict the possible (meta)stable polymorphs of a chemical compound.[1−4] The knowledge of the existence of a (meta)stable compound and its structure is important in order to plan the synthesis of new materials, and to study their properties under standard and extreme conditions.[2,3]

The starting point of most structure prediction methods is the fact that (meta)stable modifications of chemical systems correspond to locally ergodic regions[5,6] of the energy landscape.[5,7] The latter notion is a refinement of ergodicity: a system is ergodic when the time average is identical to the ensemble average in the limit of time approaching infinity. Locally ergodic means that a system can equilibrate on a time scale small compared to the observation time, and the escape time from this region is large compared to the observation time. At low temperature, individual minima can be locally ergodic, if they are separated by sufficiently high energy barriers. Usually, there exist many such locally ergodic regions encompassing one or several local minima, the latter case being most important, if some of the sites in a structure are only partly occupied, or occupied in a disordered fashion.[8] While studying the energy landscape, we are interested not only in the thermodynamically stable structures but also in all kinetically sufficiently stable ones. Thus, the global exploration is not limited to the search for the global minimum but local minima[2] are also identified.

There are a number of algorithms which are used for structure prediction of solid compounds. One class are straightforward global optimization techniques, e.g., simulated annealing,[9−12] genetic/evolutionary algorithms,[13−17] or basin hopping;[18,19] another group proceeds more indirectly such as the threshold algorithm[20] or metadynamics.[21,22] Another feasible optimization technique is particle swarm optimization,[23] which has been applied, e.g., to predict protein folding using a toy model[24] or to solve crystal structures from powder diffraction.[25]

Since structure prediction is a very time consuming task involving many millions of energy calculations, one usually attempts to reduce the computational effort by employing simplified energy functions that are typically based on some empirical potentials. Such potentials are often of sufficient quality and computationally cheap as well but they have some in-principle shortcomings. They are system dependent, and even for a given system, it is not guaranteed that all relevant polymorphs correspond to basins around local minima. Furthermore, while these potentials are quite successful for ionic systems, they often encounter problems for systems with covalent or metallic bonds or mixtures thereof. As a consequence, we need to employ ab initio based energy calculations already during the global search.[26]

Several years ago, it was demonstrated that global optimization with simulated annealing[27] and genetic algorithms[16] is possible with all energy calculations perfomed on the ab initio level. For example, the ionic system lithium fluoride (LiF) was one of the first systems studied on the ab initio level[27] in order to validate the methodology. LiF had been studied with model potentials[12,28] earlier, and it was found that the most relevant minima were the same on the level of empirical potentials and on the ab initio level. Subsequently, boron nitride (BN), a covalent system, was successfully investigated using ab initio simulated annealing as the global exploration method.[29] The possibility to compute barriers was demonstrated for LiF clusters.[30]

In this study, we go one step further and investigate CaC_2, a mixed covalent-Ionic system. We note that in all experimentally known structures in this system, the carbon atoms combine to form C_2 dumbbells. Since the bonds between the carbon atoms in the dumbbells are covalent whereas the interaction between Ca and C_2 is "ionic", the global energy landscape of CaC_2 cannot be easily described by straightforward empirical potentials. Thus, it is necessary to perform the global search for structure candidates on the ab initio level. Besides allowing us to deal with complex interactions, using ab initio energies also enables us to dispense with the use of rigid C_2-building units during the global search, as had been commonly used for similar systems containing complex building blocks in the past,[31] and

* To whom correspondence should be addressed. E-mail: K.Doll@fkf.mpg.de.

10.1021/jp1028504
Published on Web 11/05/2010

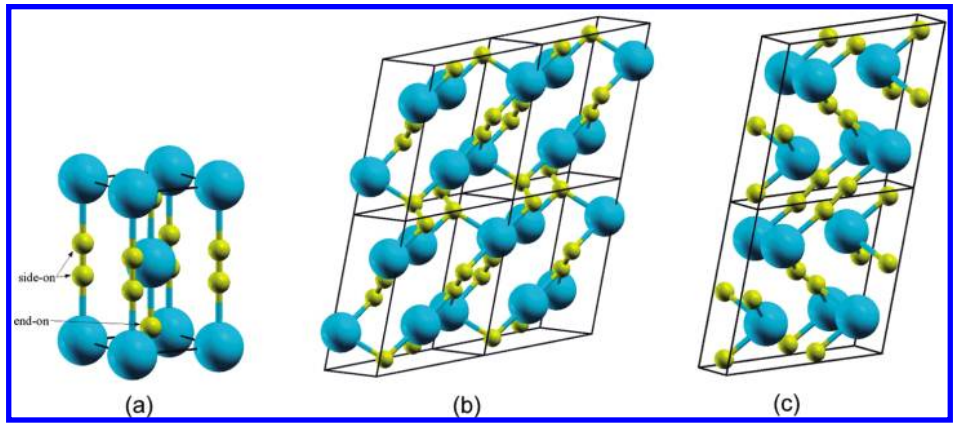

Figure 1. Experimentally known low-temperature modifications of CaC_2: (a) CaC_2-I (experimental + predicted), (b) CaC_2-II, and (c) CaC_2-III. Blue (big) spheres correspond to calcium, yellow (small) spheres to carbon atoms, respectively. The lines indicate the unit cells, with the *z*-axis pointing upward. The label "side-on" ("end-on") marks the C_2-dimer which is a side-on (end-on) neighbor of the central Ca atom.

to employ freely moving individual carbon atoms instead. In this fashion, one is able to identify structures that exhibit C-atom networks, which might possibly occur at very high pressures.

Experimentally, four different modifications of CaC_2 are known (cf. Figure 1a−c). At room temperature, CaC_2-I crystallizes in the body-centered tetragonal system with space group *I*4/*mmm* (no. 139)[32] and unit cell parameters $a = 3.87$ Å and $c = 6.40$ Å. The C_2 dumbbells are oriented along the [001] axis of the structure. With the C_2 dumbbells differently orientated, there are two more modifications, viz., CaC_2-II with space group *C*2/*c* (no. 15)[32] and CaC_2-III with space group *C*2/*m* (no. 12),[32] both of which are assumed to be metastable. In both monoclinic structures, the C_2^{2-} unit is surrounded by a distorted octahedron made of Ca^{2+} ions. Finally, cubic CaC_2-IV[32] is found at high temperature. It can be visualized as a rock-salt structure with Ca^{2+} in the Na^+ positions and the center of gravity of the rotating C_2^{2-} dumbbells in the Cl^- positions. CaC_2 is commonly used for the production of acetylene.[33] There are additional applications such as desulfurization of iron,[34] production of calcium cyanamide,[35] and carbide lamps.[36]

This paper is organized as follows: the global search method is briefly explained in the next section. In the Results section, the outcome of the global explorations are presented for optimizations at standard and elevated pressures. In the Discussion section, the results are compared with the experimentally observed CaC_2 polymorphs and typical AX_2-type structures found in other chemical systems. Furthermore, the effect of the rotation of the C_2 dumbbell in all directions is analyzed, which plays an important role in understanding the stability of this material. Finally, the performance of the global optimization algorithm used is discussed.

Method

General Approach. The exploration of the landscape can be broadly divided into two steps, viz., global optimization and local optimization. First, a global optimization method is employed for the determination of a structure candidate. Next, the symmetry and space group of the candidate is determined. Then, this candidate is locally optimized, and again, the symmetry and space group are identified. A large number of such global searches are performed in order to obtain many different structure candidates, and to gain some statistics about how often each structure was found. During the global and local optimization, no atoms were frozen and a full optimization of all parameters was performed (unit cell, atom positions). The results of these local optimizations are used to draw E−V (energy−volume) curves for the various modifications. By calculating the enthalpies for the various structure candidates, one can determine the transition pressures between different modifications by setting the enthalpies equal. One should note that the procedure described does not identify disordered structures with partially occupied sites or, e.g., rotating complex anions/cations. To find such modifications, an additional extensive analysis of the data and typically the study of considerably larger simulation cells with more atoms are required.[8]

Details. ***Global Optimization.*** In the following paragraphs we describe technical details of the search in the calcium carbide system, starting with the global optimization. Regarding the system size, we have considered 2, 3, and 4 formula units of CaC_2 per simulation cell, where one formula unit consists of one Ca and 2 C atoms, since from databases[37] it is known that most binary crystalline structures can be described by using up to four formula units per primitive cell. At the beginning of the global optimization, these atoms were placed at random positions in the cell. The initial volume of the simulation cell was chosen using the following procedure: first, the total volume is computed based on tabulated ionic radii for the atoms, and then this volume is multiplied with a factor typically in the range from 3 to 5. In the system studies here, the initial volume of the simulation cell was 883 $Å^3$ in the case of 2 formula units and 2650 $Å^3$ in the case of 4 formula units (corresponding to a cube with side length of 9.59 and 13.84 Å, respectively). This cell is periodically repeated; i.e., periodic boundary conditions are applied. Within this large initial volume, the atoms can arrange themselves in any configuration during the Metropolis random walk, and thus none of the basins corresponding to energetically low-lying compact structures is favored or excluded by the choice of the initial configuration.

The global optimization is based on simulated annealing and a subsequent stochastic quench. During the simulated annealing stage, the energy of a newly generated structure is computed and compared with the previous one. If the energy of the new structure is lower, then the new structure is accepted. If the energy of the new structure is higher, then the new structure is accepted with a probability of $\exp(-\Delta E/k_B T)$ (where ΔE is the energy difference between the two structures, T the temperature, and k_B the Boltzmann constant). This corresponds to the Metropolis algorithm.[38] The initial temperature for the simulated annealing was 1.00 eV (∼11 604 K) and 6250 steps are used for 2, 3, and 4 formula units. During the simulation, the temperature is exponentially reduced: after 250 steps, it is multiplied by a factor of 0.995. The temperature at the end of

TABLE 1: Total Energies at Zero Pressure of the Relaxed Structures of the Most Important Modifications Found and Their Statistics of Occurrence during the Global Optimization[a]

		energy (E_h)			number of times found (at press. in GPa)				
name of modification (struct)	space group	LDA	B3LYP	HF	0	16	32	48	64
CaC_2-I (tetragonal)	$I4/mmm$(139)	−112.1717	−112.9470	−112.2114	11	1	3	2	0
CaC_2-V (orthorhombic)	$Immm$(71)	−112.1735	−112.9499	−112.2141	18	3	3	5	1
CaC_2-VI (monoclinic)	$C2/m$(12)	−112.1720	−112.9481	−112.2125	5	1	0	1	1
CaC_2-VII (trigonal)	$R\bar{3}m$(166)	−112.1532	−112.9215	−112.1821	0	2	4	1	4
other modifications[b]					20	0	2	4	1
no. of successful runs					54	7	12	13	7
total no. of runs					227	24	24	32	24

[a] Energies are in hartree units (1 E_h = 27.2114 eV), per formula unit. A run is termed as successful if it reaches a stable local minimum structure. Out of 227 runs at standard pressure 54 were successful. Similarly, among the 104 runs at elevated pressures, there were 39 successful runs. [b] With higher energies and irregular polyhedra.

a simulated annealing run was 0.88 eV (~10 245 K). After the simulated annealing, a quench was applied, i.e., a simulated annealing run with the temperature 0 eV. The simulated annealing and quench moves were selected as follows: movements of individual atoms, atom exchange, and change in lattice parameters were attempted 70%, 10%, and 20% of the time, respectively. When applying moves that change one of the lattice constants, the probability to shrink the lattice constant was set to 60%, in order to accelerate the shrinking of the cell. We note that extending the length of the simulated annealing run phase of the global optimization to 15 000 steps did not lead to significant changes.

The calculations were repeated for a number of pressures (0, 16, 32, 48, and 64 GPa) in order to search for possible high-pressure polymorphs.

Other important parameters are the minimum allowed distance between two atoms and the reduction of the cell size. The minimum distance between two atoms was required to be 0.7 times the sum of the ionic radii in order to avoid unphysical geometries which can cause numerical instabilities in the ab initio calculations (see below). In order to estimate the atomic/ionic radii, first a Mulliken population analysis was performed. Then, the atomic and ionic radii were obtained from tabulated values of the corresponding atoms/ions, as a function of charge[39] (and employing a simple linear interpolation to obtain the radii, as the computed Mulliken charges are noninteger). We note that there is an ongoing discussion concerning the accuracy of the Mulliken population analysis[40−43] However, we do not expect a big impact of the accuracy of the Mulliken population on the present calculations, as the derived charges and radii are only used to eliminate very unrealistic conformations.

Analyses of Structure Candidates. Typically, the structure candidates will not show any symmetries after the global search: they are given in space group $P1$, due to the unrestricted optimization procedure. To deal with this issue, we use two algorithms to search for symmetries (SFND)[44] and to determine the space group (RGS),[45] respectively, which are implemented in the program KPLOT.[46] Furthermore, we used the CMPZ algorithm (designed to compare two periodic structures),[47] as implemented in KPLOT, to eliminate duplicates and to compare the candidates with the structures found experimentally. After the global and local optimization, the symmetry is identified, and the structural data is expressed in the corresponding space group, and only the position of the irreducible atoms is required, reducing the number of parameters needed to describe the structure. This accelerates the local optimization considerably.

Local Optimization. The local optimization is performed using analytical gradients,[48−52] taking the symmetry of the structure into account. In order to gain an estimate of the validity of the ab initio calculations, we have performed both Hartree−Fock and DFT (local density approximation, LDA, and the hybrid functional, B3LYP) calculations for all structures and systems during the local optimization. This local optimization is performed at zero temperature. These calculations require little CPU time and are therefore done with high-accuracy computational parameters.

Energy Calculations. All energy calculations during the global search were performed on ab initio level with periodic boundary conditions using the CRYSTAL06 code.[53] It is based on local Gaussian-type orbitals. Two basis sets were used for the optimization (see the Appendix). We note that the ab initio total energy calculations for the global optimization were performed on the Hartree−Fock level, since the Hartree−Fock calculations are easier to converge for insulators due to the resulting larger size of the band gaps compared to DFT calculations. This is especially important as the atoms initially are at random positions that can be quite far apart.[29]

Keeping the CPU time low plays a key role in the efficieny of the global search. This requires a careful calibration of many parameters in simulated annealing, e.g., the initial volume and temperature, the number of simulation steps and cooling schedule, and the parameters of the ab initio energy calculations. The initial volume and temperature are very large; i.e., the system is essentially in a gaseous state at the start. Converging the total-energy calculation both at such a random geometry and at all later stages of the simulated annealing and the quench is a particularly difficult task for the system CaC_2 due to the mixed (covalent−ionic) nature of the bonds.

In order to speed up the calculations during the global search, the self-consistent field cycles were terminated when the energy difference between two consecutive cycles was 10^{-4} E_h. A k-point mesh of the size 4 × 4 × 4 was used. In contrast, for the local optimization, default convergence criteria (10^{-7} E_h) and a larger k-point mesh (8 × 8 × 8) were used.

Results

Standard Pressure. For standard pressure, we performed 227 global optimization runs. As a result, we obtained 10 different structure candidates for this system with space group different from $P1$. All polymorphs found showed the formation of C_2 bonds from initially widely separated carbon atoms. We found three modifications denoted CaC_2-I, -V, and -VI, which are energetically particularly stable (low-lying) at standard pressure. The total energies of these structures, after the local optimization, are displayed in Table 1. These predicted structures are depicted in Figures 1a and 2a,b with XCRYSDEN,[54] and their optimized structures are given in Table 2. In all structures, the carbon atoms

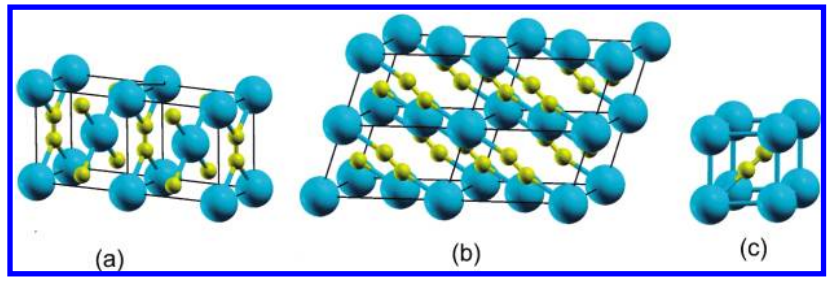

Figure 2. Newly predicted low-temperature modifications of CaC_2. For notation cf. Figure 1. Modifications (a) CaC_2-V and (b) CaC_2-VI are low-pressure modifications; (c) CaC_2-VII is a high-pressure modification.

TABLE 2: Energetically Most Favorable Structures in the CaC_2 System, Plus Several Structures at Higher Energy Derived from Well-Known Structure Types

	cell parameters and fractional coordinates		
modification and space group	predicted, LDA	exptl at 83 K[32]	energy (hartrees) per formula unit (LDA)
CaC_2-I(expt)		$a = 3.87$ Å, $c = 6.40$ Å	
CaC_2-I(predicted)	$a = 3.87$ Å, $c = 6.34$ Å		−112.1717
*I*4/*mmm*(139)	Ca(0, 0, 0)	Ca(0, 0, 0)	
tetragonal structure	C(0, 0, 0.399)	C(0, 0, 0.407)	
CaC_2-V(predicted)	$a = 3.71$ Å, $b = 5.34$ Å, $c = 4.89$ Å		−112.1735
Immm(71)			
orthorhombic structure	Ca(0,0,0)		
	C(0, 1/2, 0.130)		
CaC_2-VI(predicted)	$a = 6.85$ Å, $b = 3.88$ Å,		−112.1720
*C*2/*m*(12)	$c = 3.95$ Å		
monoclinic structure	$\beta = 114.3°$,		
	Ca(0,0,0)		
	C(0.595, 0.000, 0.628)		
CaC_2-II(expt)[a]	$a = 6.56$ Å, $b = 4.11$ Å	$a = 6.60$ Å, $b = 4.19$ Å	−112.1732
*C*2/*c*(15)	$c = 7.60$ Å	$c = 7.31$ Å	
monoclinic structure	$\beta = 109.1°$	$\beta = 107.0°$	
	Ca(0, 0.325, 1/4)	Ca(0, 0.182, 1/4)	
	C(0.230, 0.145, 0.935)	C(0.282, 0.146, 0.056)	
CaC_2-III(expt)[a]	$a = 7.05$ Å, $b = 3.80$ Å	$a = 7.21$ Å, $b = 3.83$ Å	−112.1731
*C*2/*m*(12)	$c = 7.52$ Å	$c = 7.37$ Å	
monoclinic structure	$\beta = 106.6°$	$\beta = 107.2°$	
	Ca(0.204, 0.000, 0.249)	Ca(0.197, 0, 0.254)	
	C1(0.542, 0.000, 0.935)	C1(0.421, 0, 0.021)	
	and C2(0.080, 0.000, 0.566)	and C2(0.952, 0, 0.420)	
CaC_2-VII(predicted)	$a = b = c = 3.51$ Å		−112.1532
$R\bar{3}m$(166)	$\alpha = \beta = \gamma = 86.6°$		
trigonal structure	Ca(0, 0, 0)		
	C(0.600, 0.600, 0.600)		
"$Ca(CN_2)$" configuration	$a = b = c = 4.55$ Å		−112.1678
$R\bar{3}m$(166)	$\alpha = \beta = \gamma = 49.4°$		
trigonal structure	Ca(0, 0, 0)		
	C(0.447, 0.447, 0.447)		
"Cu(NCN)" configuration	$a = b = 3.78$ Å, $c = 8.09$ Å		−112.1653
$P6_3/mmc$(194)	$\gamma = 120.0°$		
hexagonal structure	Ca(0, 0, 0)		
	C(1/3, 2/3, 0.328)		
FeS_2 (pyrite) configuration	$a = b = c = 5.81$ Å		−112.1654
$Pa\bar{3}$(205)	Ca(0, 0, 0)		
cubic structure	C(0.437, 0.437, 0.437)		
MgC_2 configuration	$a = b = 6.42$ Å, $c = 2.93$ Å		−111.7925
$P4_2/mnm$(136)	Ca(0, 0, 0)		
tetragonal structure	C(0.730, 0.730, 0)		

[a] Not found in the structure prediction, but instead experimental data was optimized.

form isolated dumbbells. The computed C−C bond length ranges from 1.272 Å to 1.280 Å for the low temperature structures CaC_2-I to -VI and CaC_2-VII (see Table 3, where the bond lengths after the local optimization are displayed).

The first predicted structure candidate was identical with the experimentally observed tetragonal structure (CaC_2-I),[55,56] which is the room temperature modification. C_2 dumbbells point along the [001] axis of the tetragonal unit cell (see Figure 1a). Each Ca atom is surrounded by 4 C_2 units in a side-on way and 2 C_2 units in an end-on way.

From our simulation, we predicted two additional low-energy structures labeled as CaC_2-V and CaC_2-VI. In CaC_2-V (see Figure 2a), the C_2 dumbbells are oriented along the [001] axis. Two C_2 units are side-on to Ca atoms. This breaks the tetragonal symmetry when compared to CaC_2-I; i.e., the C_4 axis of rotation is missing in the CaC_2-V structure, and the space group is *Immm*.

TABLE 3: Interatomic C−C Distances (Å) and Volumes (Å^3) per Formula Unit of the Most Relevant Modifications after Local Optimization on the LDA Level at Standard Pressure

	C−C distance (in Å)		
modification	experimental	computed	volume (Å^3)
CaC_2-I	1.19	1.277	47.515
CaC_2-V		1.272	48.420
CaC_2-VI		1.274	47.805
CaC_2-II	1.19	1.274[a]	48.364[a]
CaC_2-III	1.18	1.275[a]	48.254[a]
	1.27		
CaC_2-VII		1.280	43.049

[a] Not found in the structure prediction, but instead obtained from the local optimization of experimental data.

TABLE 4: Interatomic Distances (Å) between Ca and C Atoms in the CaC_2-I, -II, -III, -V, -VI, and -VII Modifications, with Different Types of Coordination of Ca by C_2 Dumbbells at Zero Pressure after Local Optimization on the LDA Level

		distance from nearest carbon atom (Å)	
modification	coordination of Ca by C-atoms	exptl[a]	predicted
CaC_2-I	2*x*,end-on	2.531	2.531
	8*x*,side-on	2.812	2.812
CaC_2-V	4*x*,end-on		2.589
	4*x*,side-on		2.747
CaC_2-VI	2*x*,end-on		2.551
	4*x*,side-on		2.668
CaC_2-II	2*x*,end-on	2.567	
	2*x*,side-on	2.602	
	2*x*,side-on	2.756	
	2*x*,side-on	2.795	
	2*x*,side-on	3.304	
CaC_2-III	end-on	2.556	
	side-on	2.753	
	side-on	2.765	
	2*x*,end-on	2.579	
	2*x*,side-on	2.676	
	2*x*,side-on	2.990	
CaC_2-VII	2*x*,end-on		2.576
	6*x*,side-on		2.813

[a] After local optimization of experimental data.

Although the predicted CaC_2-VI polymorph shows the same space group as CaC_2-III, the two structures are not the same. This is most obvious from the fact that CaC_2-VI requires only two formula units per primitive cell, while CaC_2-III contains 4 formula units per primitive cell. In CaC_2-VI (see Figure 2b), the Ca_6-octahedra around the C_2 dumbbells are strongly distorted. Each Ca atom is surrounded by 2 end-on and 4 side-on C_2 dumbbells.

The experimental low-temperature modification CaC_2-III[56] is displayed in Figure 1c. The LDA-optimized C−C distance in the C_2 dumbbell is about 1.275 Å. Again, the C_2 dumbbells are surrounded by a Ca_6-octahedron. Each Ca atom is enclosed by 3 C atoms in an end-on way and 6 C atoms in a side-on way. For completeness, we describe the modification CaC_2-II.[56] It takes the form of the ThC_2 structure type[57] with C_2 dumbbells directed toward an edge of a Ca_6-octahedron and a small tilt angle. The octahedron itself is very strongly distorted (see Figure 1b). In CaC_2-II, a Ca atom is enclosed by 4 side-on and 2 end-on C_2 dumbbells (Table 4).

Elevated Pressure. We have carried out 104 global optimization runs for the following high pressures, viz., 16, 32, 48, and 64 GPa (cf. Table 1). One of the most striking results of the landscape investigations is the persistence of major features of the energy landscape over a wide pressure range. Besides some of the structures already observed at standard pressure, several new candidates were found. For 16 GPa, the results show CaC_2-I, CaC_2-V, CaC_2-VI, and CaC_2-VII as possible structure candidates. But at a pressure above 32 GPa, the one with the lowest enthalpy is the CaC_2-VII structure (see Figure 2c), which we predict to be the thermodynamically stable one. The crystal structure of CaC_2-VII shows similarities to the CsCl structure. The Ca atoms form a distorted cube with the C_2 units in the center (see Figure 2c) and, conversely, the centers of mass of the C_2 units form a distorted cube around the Ca atoms. Due to the distortions, the cubic symmetry of the "CsCl-type arrangement" is reduced, resulting in the space group $R\bar{3}m$ (no. 166). Our results only apply to low temperature, of course. At elevated temperatures, we expect that the C_2 units will be able to rotate freely, and thus the CaC_2-VII structure will transform to a CsCl-type structure.

The E−V curves for all relevant candidates are plotted for two different DFT functionals, viz., LDA and B3LYP (see Figure 3, a and b). When pressure is applied to the system, the high-coordinated structures become more favorable, which is in agreement with the rule that the coordination number increases with pressure; see e.g., ref 58. It is obvious from Figure 4a that the high-pressure structure would, at standard pressure, have the smallest volume per formula unit and thus the highest density, whereas CaC_2-I to -VI all have very similar volumes at standard pressure (see Table 3). The enthalpies are presented in Figure 4, a and b, for LDA and B3LYP, respectively. The transition is being observed from the structure CaC_2-VI to the structure CaC_2-VII, and the transition pressure computed with LDA and B3LYP is 24 and 34 GPa, respectively.

Discussion

Comparison with Experiment. Up to now, only standard pressure modifications of CaC_2 are available for a comparison regarding structural data. From Table 3, we see that there is good agreement between the experimentally observed bond lengths and the ones computed by theory. The exception is CaC_2-III where two significantly different bond lengths are found in experiments (1.18 and 1.27 Å at 83 K, and even 1.13 and 1.48 Å at 295 K). However, it was argued[32] that the experimental result could be an artifact of the refinement. In order to clarify this issue, we optimized the CaC_2-III structure, resulting in a bond length of 1.275 Å, which is in much better agreement with those found in the other modifications.

Both the experimentally known structures (CaC_2-I, -II, and -III) and the predicted low-temperature structures (CaC_2-I, -V, and -VI) can be derived from the rock-salt structure type: the centers of the C_2 dumbbells form an elongated and distorted octahedron around Ca atoms and, conversely, the dumbbells are in the centers of elongated octahedra of Ca atoms. The distances between Ca and the neighboring C atoms are displayed in Table 4. The main difference between these five structures is the spatial orientation of the C_2 dumbbells. This is consistent with the fact that the high-temperature modification CaC_2-IV is described in the rock-salt type, where the rotating C_2 dumbbells lie at the center of Ca-octahedra. We note that the three experimentally observed low-temperature modifications[32] are found to coexist at 295 K.[32] At a temperature of about 640 K,[32] CaC_2-II transforms to CaC_2-I and CaC_2-III.

In the present calculations, the CaC_2-V structure turns out to be the energetically most favorable structure. The energies of

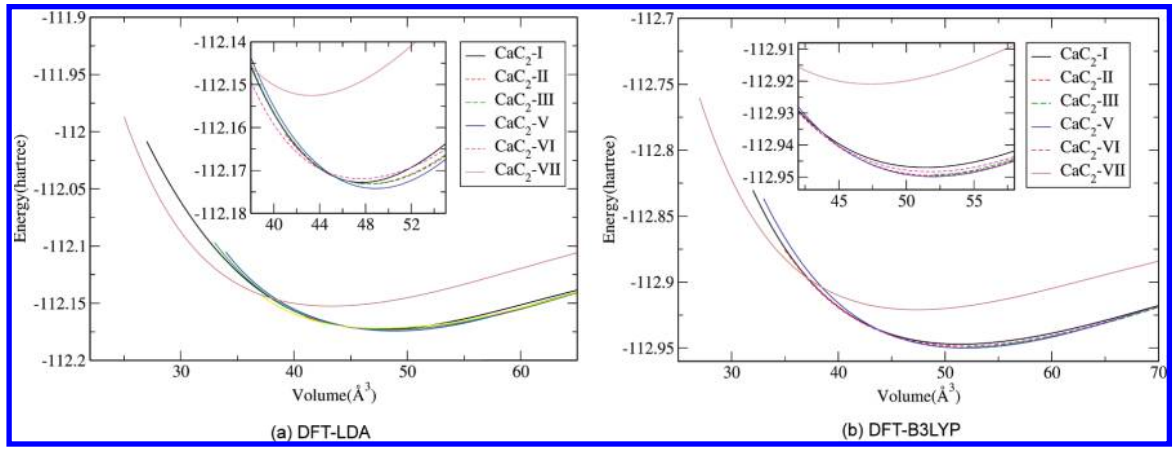

Figure 3. E−V curves of the most relevant structures, at the LDA and B3LYP level. Energies per formula unit are given in hartrees (E_h).

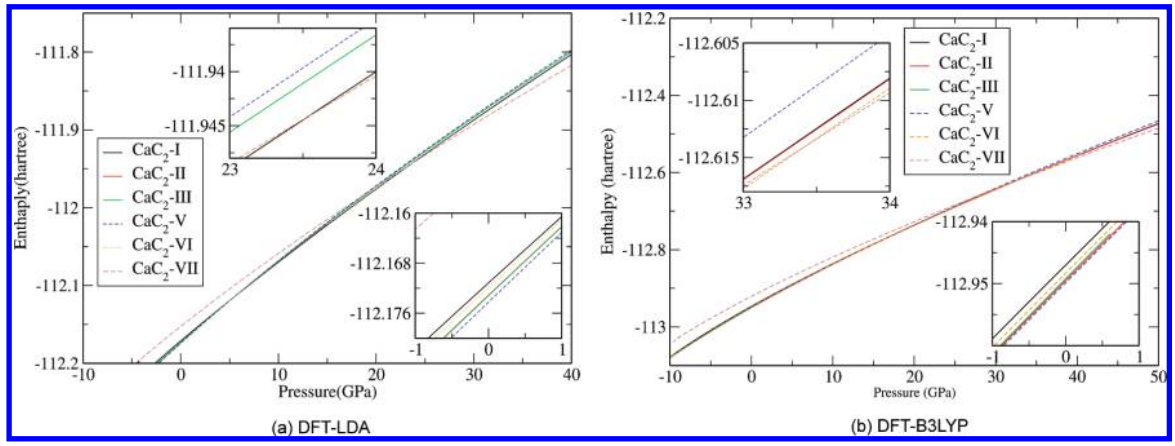

Figure 4. Enthalpies per formula unit of the most relevant structures at the LDA and B3LYP level. Inset upper left, high-pressure range; inset lower right, standard pressure range.

the experimentally observed monoclinic structures (CaC_2-II and -III) are higher by about 0.4 mE_h per formula unit (≈4 meV/atom), corresponding to about 42 K. The predicted monoclinic structure (CaC_2-VI) is higher by about 1.5 mE_h per formula unit (≈14 meV/atom, i.e., by about 160 K), and the tetragonal structure (CaC_2-I) is higher by about 1.8 mE_h per formula unit (≈16 meV/atom) corresponding to about 190 K. We suggest that all five modifications, plus additional variants with alternative C_2 orientations, should be able to exist at low temperature. In this context, we note that for the LDA functional, there is a transition from CaC_2-V to CaC_2-I at about 5 GPa and one more transition observed at about 7 GPa from CaC_2-I to CaC_2-VI (see Figures 3a and 4a) .

Analyses of the Barrier Structures. As noted above, all the structures CaC_2-I to -VI are based on an essentially cubic close packed arrangement of the Ca atoms, where the C_2 units are located in the octahedral voids. These structure types only differ with respect to the orientations of the C_2 units, leading to the many different low-temperature structures observed and predicted. In order to gain some insight into the stability of these structures, we have analyzed the effect of the rotations of the C_2 dumbbells.[59,60] Starting (and reference) configuration is the CaC_2-I structure, where we have selected one of the (equivalent) dumbbells. Each rotation of this C_2 unit is followed by a relaxation of the rest of the structure via a local optimization. The rotation of the C_2 dumbbell can be described by a zenith angle (θ) and an azimuthal angle (ϕ) (see Figure 5a). When $\phi = 0°$, each C atom points toward the opposite face of the octahedron, and for $\phi = 45°$ each carbon atom points toward the opposite edge of the octahedron.

Starting from the structure CaC_2-I and then tilting the C_2 dumbbell by a very small angle ($\theta \leq 2°$ and $\phi = 0°$), we find that the subsequent local optimization leads us back to the original structure CaC_2-I. When the tilt angle is larger ($10° \leq \theta \leq 50°$), then the structure becomes CaC_2-VI after the subsequent local optimization. When the tilt angle exceeds 60°, then the local optimization leads to the structure CaC_2-V (see Figure 5b). This result holds essentially for any angle ϕ, demonstrating how the structures CaC_2-I, CaC_2-V, and CaC_2-VI are connected on the energy landscape. In contrast, the CaC_2-II and CaC_2-III structures cannot be transformed into CaC_2-I by a simple rotation of a single C_2 unit.

An estimate of the upper bound of the barriers is possible for transitions from the tetragonal (CaC_2-I) to the monoclinic (CaC_2-VI) or the orthorhombic (CaC_2-V) structure. The starting point was the tetragonal polymorph, with the C_2 dumbbell oriented along the z-axis. Then, the C_2 dumbbell was rotated and a local optimization was performed. When the C_2 dumbbell is rotated (and no optimization performed), the energy increases monotonously with the tilt angle θ (up to $\theta = 90°$). Therefore, this energy can be used as an upper bound of the barrier. To have a transition from the tetragonal structure to the monoclinic structure, a tilt angle of 2° is required. The energy (for one formula unit) of the structure after such a tilt is 0.0001 hartree higher than that of the tetragonal structure, and this is an upper bound for the barrier. This barrier is very small; i.e., there is practically no barrier. To have a direct transition from the tetragonal to the orthorhombic structure, a tilt angle of 60° is required. The energy after such a tilt is 0.039 hartree higher than that of the tetragonal structure (for one formula unit). Again,

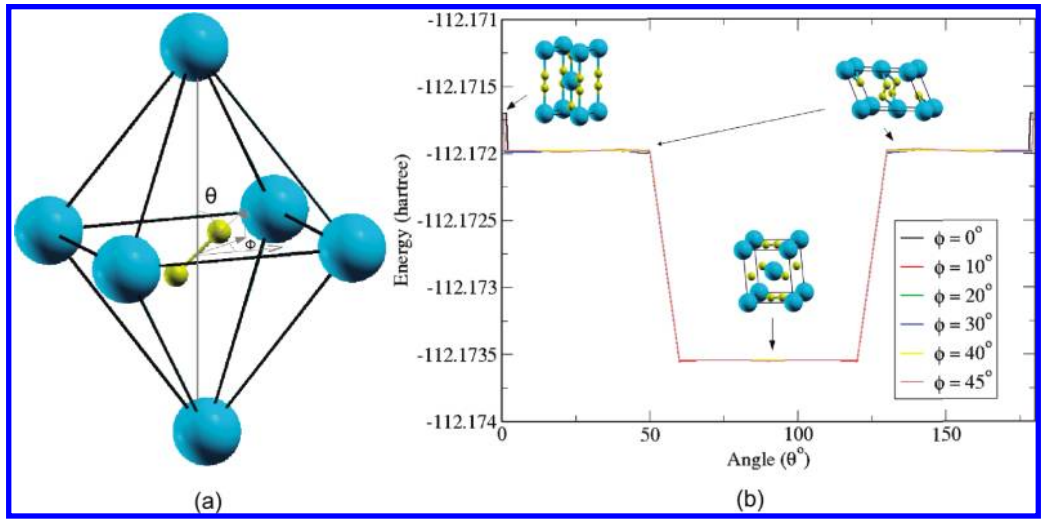

Figure 5. (a) Definition of the tilt angles θ and ϕ. (b) Rotation of the C_2 unit starting in the CaC_2-I configuration. The curve shows the energy per formula unit after tilting the C_2 dumbbell by an angle ϕ (ϕ = 0°, 10°, 20°, 30°, 40°, and 45°) and rotating by an angle θ through 180°, and subsequently performing local optimization. Three ranges of θ can be distinguished, [0°,2°], [10°,50°] and [60°,90°], belonging to the basins of the CaC_2-I, CaC_2-VI, and the CaC_2-V modifications. Note that the value of ϕ does not influence the outcome of the local minimization.

TABLE 5: Optimization of Crystal Structures Taken from ICSD (Ref 37)[a]

	before local optimization		after local optimization			
ICSD compd	structure type	space group	structure type	space group	energy	Ca_6-octahedron
BaC_2	ThC_2	*C*2/*c*	CaC_2-V	*Immm*	−112.1735	yes
$Ca(CN_2)$	high temp modificn of NaN_3	$R\bar{3}m$	high temp modificn of NaN_3	$R\bar{3}m$	−112.1678	no (approximately cubic)
Cu(NCN)		*Cmcm*		$P6_3/mmc$	−112.1653	no (NiAS type)[b]
FeS_2	marcasite	*Pnnm*	CaC_2-I	*I*4/*mmm*	−112.1717	yes
FeS_2	pyrite	$Pa\bar{3}$	pyrite	$Pa\bar{3}$	−112.1654	yes
KO_2		*C*2/*c*	CaC_2-V	*Immm*	−112.1735	yes
MgC_2		$P4_2/mnm$		$P4_2/mnm$	−111.7925	yes
NaN_3	α-NaN_3	*C*2/*m*	CaC_2-V	*Immm*	−112.1735	yes
RhN_2		*Pnnm*	CaC_2-I	*I*4/*mmm*	−112.1717	yes

[a] Complex anions and cations were replaced by C_2 units and Ca atoms, respectively. These modified structures were locally optimized using LDA. It was checked, whether the relaxed structure exhibited Ca_6-octahedra around the C_2 dumbbells. [b] Ca at the Ni place, C_2 at the As place.

this would be an upper bound of the barrier, in this case probably much larger than the real barrier.

Comparison with CaC_2 Candidates Derived from Common $A(X_2)$-Structure Types. In the literature,[37] there exist a large number of "quasi-ionic" structures $A(X_2)$ and $A(X_3)$ containing a fixed X_2 dumbbell or X_3 dumbbell. Clearly, it would be of interest to check whether these structures correspond to local minima on the energy landscape of CaC_2. Thus, we have considered several such systems. After the appropriate replacement of the A and X atoms by Ca atoms and C_2 dumbbells, we have relaxed these structures, first keeping the space group fixed and by performing subsequently a full local optimization. We studied several systems (cf. Table 5). We observed that CaC_2 derived from FeS_2 (marcasite) and RhN_2 transformed into the CaC_2-I modification, whereas those configurations based on BaC_2, KO_2, and NaN_3 relax into CaC_2-V. These five structures have in common that initially they are not related to CaC_2-I or CaC_2-V. The FeS_2 (pyrite)-based configuration remains in the same structure type, but the energy (see Table 5) is higher than those of the other structures. Thus, this structure may only exist at high temperatures; however, there it would compete with the CaC_2-IV structure. One important feature of all the above structures is that the C_2 unit is octahedrally coordinated with Ca atoms after the local optimization.

CaC_2 in the $Ca(CN_2)$ structure type is a trigonal structure both before and after local optimization, and the C_2 dumbbell is coordinated by 8 Ca-atoms and exhibits the same space group as CaC_2-VII. Below 10 GPa, this structure has a lower enthalpy than the CaC_2-VII structure; however, for higher pressure, CaC_2-VII is thermodynamically favored. In the case of Cu(NCN), the analogous CaC_2 structure transforms from an orthorhombic structure type before optimization to a distorted NiAs type after relaxation. We compared the "Cu(NCN)", "$Ca(CN_2)$", and "FeS_2 (pyrite)" type modifications with several of those found during the global search, i.e., CaC_2-VII, CaC_2-V, and CaC_2-I, with regard to the enthalpy as function of pressure (see Figure 6). We observed that none of the modifications derived from the literature structures is thermodynamically stable compared to the predicted structures, at least at low temperatures. Thus, we conclude that our global search succeeded in identifying the relevant thermodynamically stable low-temperature structures.

Analysis of the Performance of the Global Optimization Procedure. So far, we have analyzed the outcome of the global search for possible modifications from a physical/chemical point of view by comparison with experiment and typical $A(X_2)$ structure types known from other chemical systems. We could conclude that we have most likely found the global minimum on the ab initio energy landscape investigated, and in addition a typical sample of the many possible low-energy modifications that can be generated by varying the orientation of the C_2 units.

Clearly, by performing additional simulated annealing runs, one would reach those minima too. In general, the finite computation time available limits the volume of configuration

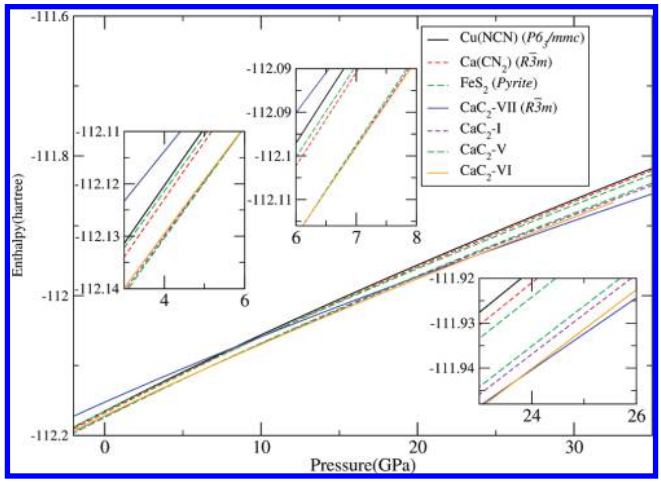

Figure 6. Enthalpy per formula unit of the three most relevant structures found during the global search and three additional ones based on well-known structure types, at the LDA level. Inset: upper left, 3−6 GPa; middle, 6−8 GPa; lower right, 23−26 GPa.

TABLE 6: Statistical Analysis at Different Pressures

pressure	no. of runs for one event	no. of event	low-lying struct	duplicates	not low-lying struct
0	10	1	1	1	8
		2	3	1	6
		3	3	1	6
		4	1	0	9
		5	2	0	8
		6	2	1	7
	100	1	3	20	77
		2	3	16	81
		3	3	15	82
high	10	1	2	2	6
		2	4	1	5
		3	3	3	4
		4	4	2	4
	100	1	4	35	61
		2	3	38	59

space that can be explored using stochastic global optimization techniques, and, in principle, the cooling should be logarithmically slow.[61,62] However, the question arises, how large an additional computational effort would be needed to substantially increase the number of new minima found, and whether this would be the most efficient use of computer resources.

In order to address this issue, we have performed an a posteriori statistical analysis concerning the structures found. The calculation of posterior probability distribution functions had been suggested as a possible statistical analysis tool.[63−66] In the present work, in order to perform a statistical analysis, we sample subsets (called events) of the total set of runs (227 at standard pressure), each subset containing 10 randomly selected runs from among the total set. For each event, the 10 runs were categorized into 3 groups, viz., low-lying structure, duplicate, and not-a-low-lying structure. The term low-lying structure is used when at the end of the run one of the energetically most favorable polymorphs is obtained. Other modifications (with higher energies and irregular coordination polyhedra) and unsuccessful runs are placed into the category not-a-low-lying structure. If one of the runs ends up in a low-lying structure which had already been observed at the event under consideration, then it is counted as a duplicate. Six such events were analyzed, and the outcome is given in Table 6. The same analysis was repeated for three events consisting of 100 randomly chosen runs out of the total of 227 runs (cf. Table 6).

We observe that out of 10 runs, 1−3 (average 2) different low-lying structures were found. Similarly, out of 100 runs, 3 (average 3) different low-lying structures were found, and the number of duplicates substantially increases. From this observation, we conclude that a substantially higher effort would be needed to find new low-lying minima.

We also performed the same statistical analysis at high pressure (16−64 GPa) using 10 and 100 (cf. Table 6) global optimization runs as events. We observe that out of 10 runs, 2−4 (average 3.25) and out of 100 runs, 3−4 (average 3.5) different low-lying structures are found, respectively, and the number of duplicates again substantially increases when moving from 10 to 100 run events. Again, we can conclude that finding new low-lying minima would require a substantially larger computational effort.

Obviously, this statistical analysis can only serve as a rough estimate on the success rate of the global optimization procedure. But there is a clear trend that considerably more runs would be needed to identify additional relevant minima. However, since the structures of these minima apparently are all variants of a common structural theme (6-/8-fold coordination of Ca by C_2 units), performing further full global optimization runs does not appear to be very efficient. Instead, new minima could be generated systematically by selectively rotating C_2 units in the basic (rock salt/CsCl) structure, and then performing local optimizations to find the corresponding local minima.

For general comparison purposes, we have also performed 64 quench runs from random starting points. Such a set of stochastic local minimizations can serve as a reference for the efficiency of the global optimization procedure. However, in the present example, none of these runs reached one of the low-lying minima, demonstrating that the simulated annealing stage of the global search is definitely necessary.

Conclusions

It was shown that structure prediction, on the basis of simulated annealing as global optimization technique and ab initio energy calculation in all steps of the search procedure, is feasible for the mixed covalent−ionic system CaC_2. The search was restricted insofar as the structures with partially occupied sites or disordered structures were not included, and also structures with a very large number of formula units in the primitive cell (>4) could not be encountered. In all polymorphs found, the carbon atoms had combined to form C_2 units. Two new structures are predicted to be at least metastable at standard pressure: an orthorhombic structure (CaC_2-V), which was found to have the lowest energy of all structures considered, and another monoclinic modification (CaC_2-VI). At high pressure (above approximately 30 GPa), a transition is predicted from the quasi-6-fold coordinated structures to a quasi-8-fold coordinated structure (CaC_2-VII) which is a distorted variant of the CsCl structure-type.

Appendix: Description of Basis Set and Pseudopotential

In the global optimization, calcium with a large core effective potential[67] was used together with a [1s] basis set. For the [1s] contraction we used the first two exponents of the [1s] contraction as it was originally calibrated together with the pseudopotential.[68] For carbon, we used a [3s2p] basis set, which was derived from the 6-31G basis set,[69] but with the outermost diffuse sp exponent replaced by 0.25, in order to speed up the calculation, and to achieve a higher numerical stability. In the subsequent local optimizations we used a small-core pseudopotential[70] for calcium, together with a [3s2p] basis set. The

tight [2s] and [2p] functions of this basis set were the same as in ref 70 and one additional s-function (0.2) was added. For carbon, we used the same basis set as in the global search, but the outermost diffuse exponent was kept at the value 0.168 714 instead of 0.25.

References and Notes

(1) Cohen, M. L. *Nature* **1989**, *338*, 291–292.
(2) Schön, J. C.; Jansen, M. *Angew. Chem., Int. Ed.* **1996**, *35*, 1286–1304.
(3) Jansen, M. *Angew. Chem., Int. Ed.* **2002**, *41*, 3746–3766.
(4) Woodley, S. M.; Catlow, C. R. A. *Nat. Mater.* **2008**, *7*, 937–946.
(5) Schön, J. C.; Jansen, M. *Z. Kristallogr.* **2001**, *216*, 307–325, 361−383.
(6) Schön, J. C.; Jansen, M. *Mater. Res. Soc. Proc.* **2005**, *848*, FF7.1.1–FF7.1.12.
(7) Schön, J. C.; Jansen, M. *Int. J. Mater. Res.* **2009**, *100*, 135–152.
(8) Schön, J. C.; Jansen, M. In *Materials Research Society Symposium Proceedings. Vol 848: Solid State Chemistry of Inorganic Materials V*; Li, J., Brese, N. E., Kanatzidis, M. G., Jansen, M., Eds.; Materials Research Society: Warrendale, PA, 2005.
(9) Kirkpatrick, S.; Gelatt, C. D., Jr.; Vecchi, M. P. *Science* **1983**, *220*, 671–680.
(10) Czerny, V. *J. Optim. Theory Appl.* **1985**, *45*, 41–51.
(11) Pannetier, J.; Bassas-Alsina, J.; Rodriguez-Carvajal, J.; Caignart, V. *Nature (London)* **1990**, *346*, 343–345.
(12) Schön, J. C.; Jansen, M. *Comput. Mater. Sci.* **1995**, *4*, 43–58.
(13) Holland, J. *Adaptation in Natural and Artificial Systems*; MIT Press: Cambridge, MA, 1992.
(14) *Applications of Evolutionary Computation in Chemistry*; Johnston, R. L., Ed.; Springer: Berlin, 2004.
(15) Woodley, S. M.; Battle, P. D.; Gale, J. D.; Catlow, C. R. A. *Phys. Chem. Chem. Phys.* **1999**, *1*, 2535–2542.
(16) Oganov, A. R.; Glass, C. W. *J. Chem. Phys.* **2006**, *124*, 244704–244718.
(17) Woodley, S. M. *Phys. Chem. Chem. Phys.* **2007**, *9*, 1070–1077.
(18) Nayeem, A.; Vila, J.; Scheraga, H. A. *J. Comput. Chem.* **1991**, *12*, 594–605.
(19) Wales, D. J.; Doye, J. P. K. *J. Phys. Chem. A.* **1997**, *101*, 5111–5116.
(20) Schön, J. C.; Putz, H.; Jansen, M. *J. Phys.: Condens. Matter* **1996**, *8*, 143–156.
(21) Laio, A.; Parrinello, M. *Proc. Natl. Acad. Sci. U.S.A.* **2002**, *99*, 12562–12566.
(22) Martonak, R.; Laio, A.; Parrinello, M. *Phys. Rev. Lett.* **2003**, *90*, 075503−075506.
(23) Kennedy, J.; Eberhart, R. *Proc. IEEE Int. Conf. Neural Networks IV* **1995**, 1942–1948.
(24) Liu, J.; Wang, L.; He, L.; Shi, F. *Analysis of Toy Model for Protein Folding Based on Particle Swarm Optimization Algorithm*; Springer: Berlin, 2005.
(25) Feng, Z. J.; Dong, C.; Jia, R. R.; Deng, X. D.; Cao, S. X.; Zhang, J. C. *J. Appl. Crystallogr.* **2009**, *42*, 1189–1193.
(26) Schön, J. C.; Doll, K.; Jansen, M. *Phys. Status Solidi B* **2010**, *247*, 23–39.
(27) Doll, K.; Schön, J. C.; Jansen, M. *Phys. Chem. Chem. Phys.* **2007**, *9*, 6128–6133.
(28) Čančarević, Ž.; Schön, J. C.; Jansen, M. *Chem. Asian J.* **2008**, *3*, 561–572.
(29) Doll, K.; Schön, J. C.; Jansen, M. *Phys. Rev. B* **2008**, *3*, 144110.
(30) Doll, K.; Schön, J. C.; Jansen, M. *J. Chem. Phys.* **2010**, *133*, 024107.
(31) Mellot-Drazneks, C.; Girard, S.; Férey, G.; Schön, J. C.; Čančarević, Ž.; Jansen, M. *Chem.−Eur. J.* **2002**, *8*, 4102–4113.
(32) Knapp, M.; Ruschewitz, U. *Chem.−Eur. J.* **2001**, *7*, 874–880.
(33) *Kirk-Othmer Encyclopedia of Chemical Technology*, 3rd ed.; John Wiley and Sons, Inc.: New York, 1978.
(34) Langhammer, B. *Ullmann's Encyclopedia of Industrial Chemistry*; Wiley Interscience: Weinheim, Germany, 2003.
(35) Greenwood, N. N.; Earnshaw, A. *Chemistry of the Elements*, 2nd ed.; Butterworth-Heinemann: Oxford, UK, 1997.
(36) Clemmer, G. *American Miners' Carbide Lamps: A Collectors Guide to American Carbide Mine Lighting*; Westernlore Publications: Tucson, AZ, 1987.
(37) ICSD-Fiz-Karlsruhe: Inorganic Crystal Structure Database, http://icsdweb.fiz-karlsruhe.de, 2005.
(38) Metropolis, N.; Rosenbluth, A. W.; Rosenbluth, M. N.; Teller, A. H.; Teller, E. *J. Chem. Phys.* **1953**, *21*, 1087–1092.
(39) Emsley, J. *The Elements*; Oxford University Press, Inc.: Oxford, UK, 1992.
(40) Szabo, A.; Ostlund, N. S. *Modern Quantum Chemistry*; Free Press: New York, 1983.
(41) Singh, U. C.; Kollman, P. A. *J. Comput. Chem.* **1984**, *5*, 129–145.
(42) Chirlian, L. E.; Francl, M. M. *J. Comput. Chem.* **1987**, *8*, 894–905.
(43) Marynick, D. S. *J. Comput. Chem.* **1997**, *18*, 955–969.
(44) Hundt, R.; Schön, J. C.; Hannemann, A.; Jansen, M. *J. Appl. Crystallogr.* **1999**, *32*, 413–416.
(45) Hannemann, A.; Hundt, R.; Schön, J. C.; Jansen, M. *J. Appl. Crystallogr.* **1998**, *31*, 922–928.
(46) Hundt, R. *KPLOT: A Program for Plotting and Investigation of Crystal Structures*; University of Bonn: Bonn, Germany, Version 9, 2007.
(47) Hundt, R.; Schön, J. C.; Jansen, M. *J. Appl. Crystallogr.* **2006**, *39*, 6–16.
(48) Doll, K.; Saunders, V. R.; Harrison, N. M. *Int. J. Quantum Chem.* **2001**, *82*, 1–13.
(49) Doll, K. *Comput. Phys. Commun.* **2001**, *137*, 74–88.
(50) Doll, K.; Dovesi, R.; Orlando, R. *Theor. Chem. Acc.* **2004**, *122*, 394–402.
(51) Doll, K.; Dovesi, R.; Orlando, R. *Theor. Chem. Acc.* **2006**, *115*, 354–360.
(52) Civalleri, B.; D'Arco, P.; Orlando, R.; Saunders, V. R.; Dovesi, R. *Chem. Phys. Lett.* **2000**, *348*, 131–138.
(53) Dovesi, R.; Saunders, V. R.; Roetti, C.; Orlando, R.; Zicovich-Wilson, C. M.; Pascale, F.; Civalleri, B.; Doll, K.; Harrison, N. M.; Bush, I. J.; D'Arco, P.; Llunell, M. *CRYSTAL2006*; University of Torino: Torino, Italy, 2006.
(54) Kokalj, A. *Comput. Mater. Sci.* **2003**, *28*, 155–168.
(55) Reckeweg, O.; Baumann, A.; Mayer, H. A.; Glaser, J.; Meyer, H. J. *Z. Anorg. Allg. Chem.* **1999**, *625*, 1686–1692.
(56) Ruschewitz, U. *Coord. Chem. Rev.* **2003**, *244*, 115–136.
(57) Hunt, E. B.; Rundle, R. E. *J. Am. Chem. Soc.* **1951**, *73*, 4777–4781.
(58) Müller, U. *Inorganic Structural Chemistry*, 2nd ed.; Wiley: Chichester, UK, 2007.
(59) Ruiz, E.; Alemany, P. *J. Phys. Chem.* **1995**, *99*, 3114–3119.
(60) Long, J. R.; Hoffmann, R.; Meyer, H. J. *Inorg. Chem.* **1992**, *31*, 1734–1740.
(61) Geman, S.; Geman, D. *IEEE Trans. Pattern Anal.* **1984**, *6*, 721–741.
(62) Mosegaard, K.; Sambridge, M. *Inverse Prob.* **2002**, *18*, 29–54.
(63) Mosegaard, K. *Inverse Prob.* **1998**, *14*, 405–426.
(64) Alvarez, J. P. F.; Martínez, J. L. F.; Pérez, C. O. M. *Math. Geosci.* **2008**, *40*, 375–408.
(65) Armstrong, N.; Hibbert, D. B. *Chemom. Intell. Lab. Syst.* **2009**, *92*, 194–210.
(66) Armstrong, N.; Hibbert, D. B. *Chemom. Intell. Lab. Syst.* **2009**, *92*, 211–220.
(67) Fuentealba, P.; v. Szentpaly, L.; Preuss, H.; Stoll, H. *J. Phys. B* **1985**, *18*, 1287–1296.
(68) Poppe, J. http://www.theochem.uni-stuttgart.de/cgi-bin/pseudopotentiale.pl.
(69) Hehre, W. J.; Ditchfield, R.; Pople, J. A. *J. Chem. Phys.* **1972**, *56*, 2257–2261.
(70) Kaupp, M.; Schleyer, P. v. R.; Stoll, H.; Preuss, H. *J. Chem. Phys.* **1991**, *94*, 1360–1366.

JP1028504